

A General Drag Coefficient for Flow over a Sphere

Narendra Singh ¹†, Michael Kroells ², Chenxi Li ³, Eric Ching ¹,
Matthias Ihme ¹, Christopher J. Hogan ³, and Thomas
Schwartzentruber ²

¹Department of Mechanical Engineering, Stanford University, Stanford, CA 94305, USA

²Department of Aerospace Engineering and Mechanics, University of Minnesota, Minneapolis, Minnesota 55455, USA,

³Department of Mechanical Engineering, University of Minnesota, Minneapolis, Minnesota 55455, USA

(Received xx; revised xx; accepted xx)

A generalized physics-based expression for the drag coefficient of spherical particles moving in a fluid is derived. The proposed correlation incorporates essential rarefied physics, low-speed hydrodynamics, and shock-wave physics to accurately model the particle-drag force for a wide range of Mach and Knudsen numbers (and therefore Reynolds number) a particle may experience. Owing to the basis of the derivation in physics-based scaling laws, the proposed correlation embeds gas-specific properties and has explicit dependence on the ratio of specific heat capacities at constant pressure and constant volume. The correlation is applicable for arbitrary particle relative velocity, particle diameter, gas pressure, gas temperature, and surface temperature. Compared to existing drag models, the correlation is shown to more accurately reproduce a wide range of experimental data. Finally, the new correlation is applied to simulate dust particles' trajectories in high-speed flow, relevant to a spacecraft entering the Martian atmosphere. The enhanced surface heat flux due to particle impact is found to be sensitive to the particle drag model.

Key words: Authors should not enter keywords on the manuscript, as these must be chosen by the author during the online submission process and will then be added during the typesetting process (see <http://journals.cambridge.org/data/relatedlink/jfm-keywords.pdf> for the full list)

1. Introduction

An understanding of particle and droplet migration in high-speed aerospace flows is important in quantitatively describing a number of engineered systems. In particular, for high-speed flight vehicles, dust particles, water droplets in the atmosphere, or spalling fibers from the vehicle's surface may alter surface heating rates (Ching *et al.* 2020) and erode the heat shield's surface. This is particularly relevant for future Mars and Earth entry missions, where particulate matter due to dust storms (Fernández 1997), droplets or ice crystals may be present. Particle based coating processes, including cold spray deposition (Schmidt *et al.* 2006), plasma spray deposition (Herman 1988), and

† Email address for correspondence: narsingh@stanford.edu

aerosol deposition (Akedo 2006), all involve the acceleration of particles to supersonic speeds, followed by inertial impaction of the desired particles with a substrate. The quality and resulting properties of the coating are strongly dependent on the particle size and particle impaction velocity. In monitoring particle trajectories in high speed environments, accurate drag force calculations are essential; finite particle inertia yields appreciable velocity differences between particles and the surroundings at shock fronts and near surfaces. However, even if high speed gas flows are in the continuum regime, the flow relative to the motion of the particle may be in the rarefied regime. Building upon prior theoretical work in understanding drag on a spherical particle in low to high speed, and continuum to rarefied flows, the purpose of this work is to develop a physics-based expression for the drag coefficient, applicable under very general conditions, i.e. over a wide range of Mach (M_∞) number and Knudsen (Kn_∞) number (and hence Reynolds number $Re_\infty \propto M_\infty/Kn_\infty$).

In principle, drag force (F_d) on a particle of radius R depends on the free-stream relative velocity between the particle and the fluid (U_∞), density (ρ_∞), viscosity (μ_∞), temperature (T_∞) of the fluid, and surface temperature (T_w) of the particle. The coefficient of drag is defined as:

$$C_d = \frac{F_d}{\frac{1}{2}\rho_\infty U_\infty^2 \pi R^2} \quad (1.1)$$

While for restricted ranges of Re_∞ , M_∞ or Kn_∞ , theoretical estimation of drag correlation is possible, generalizations have relied on *ad-hoc* interpolations (Henderson 1976; Loth 2008) between different regimes or neural network based empirical formulations (Li *et al.* 2019). Intermediate regimes encompass a range of physical mechanisms, such as inertial effects at high Re_∞ , viscous effects at low Re_∞ , strong gas compression across shock-waves in high-speed (or high M_∞) flows, and non-continuum effects due to fewer inter-molecular collisions and wall-gas collisions in the rarefied regime ($Kn_\infty > 1.0$). In this work, we develop a physics-based generalized drag correlation by successively incorporating the contribution of these complex mechanisms through consistent physical analysis. The parameters introduced in the scaling laws are then obtained using available experimental measurements and first-principles based simulation data. One feature of the proposed correlation is its explicit dependence on the gas-type, specifically on the ratio of specific heat capacities at constant pressure and volume, which is absent in state-of-the-art correlations. We apply the proposed correlation to simulate high-speed dusty flow over a sphere to show that the surface heating rate is sensitive to the drag correlation used for estimating trajectories of dust particles. The current formulation is only for spherical objects, however, generalizations to other shapes are possible (Zhang *et al.* 2012).

2. Theory and Approach

Physical mechanisms and their relative contribution to the overall drag may vary depending on the flow regime. For instance, viscous forces dominate drag force for low Re_∞ , while inertial forces dominate as Re_∞ increases. In the present work, the flow regimes are divided based on compressibility and rarefaction effects. The Mach number (M_∞) demarcates regimes based on compressibility effects such as incompressible regime ($M_\infty < 0.3$), compressible ($0.3 < M_\infty < 1.0$), supersonic ($M_\infty > 1.0$), and hypersonic regime ($M_\infty > 5.0$). Similarly, rarefaction effects are characterized by the Knudsen number (Kn_∞), which is defined as the ratio of mean free path to the characteristic

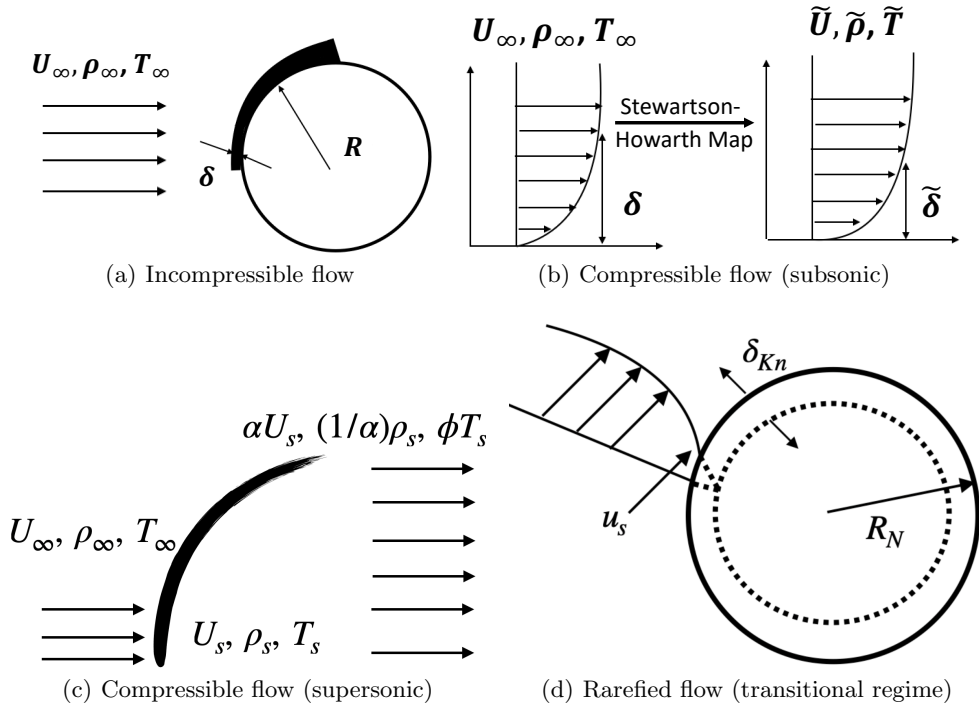


FIGURE 1. Flow over sphere in different flow regimes depicting correlation development approach

length scale ($2R$). Kn_∞ can also be expressed in terms of M_∞ and Re_∞ as:

$$Kn_\infty = \frac{M_\infty}{Re_\infty} \sqrt{\frac{\gamma\pi}{2}} \quad (2.1)$$

Low Kn ($Kn < 0.01$) corresponds to the continuum regime, followed by slip regime ($0.01 < Kn < 0.1$), transition regime ($1 < Kn < 10$) and free-molecular regime ($Kn > 10$). In the following subsections, the aforementioned flow regimes are considered and physics-based scaling laws for a generalized drag correlation are derived.

2.1. Continuum Regime Formulation

In this section, we consider the continuum regime ($Kn < 0.01$) for any M_∞ , provided that Re_∞ remains less than the critical transition condition, $Re_{\infty,c} \leq 10^4$ (i.e. before the onset of boundary layer turbulence effects). In terms of organization, incompressible flow is considered first, followed by compressible flow, which is further divided into subsonic, supersonic, and hypersonic regimes.

Incompressible flow: For sufficiently high Re ($\gg 1$), as viscous forces are confined within a thin region called the boundary layer near the wall, Abraham (1970) considered drag force on an effective sphere (of radius $R + \delta$), which includes the boundary layer (δ) region as shown in Fig. 1(a). The drag force on the effective sphere is only a function of free-stream momentum flux, and the effects of viscosity on this extended sphere can be ignored. Therefore, on the effective sphere, C_d is equal to a constant (C_0), which is

independent of Re_∞ . The drag force on the actual sphere (F_d) can then be expressed as:

$$F_d = C_0 \left(1 + \frac{\delta}{R}\right)^2 \frac{\rho_\infty \pi R^2}{2} U_\infty^2 \quad (2.2)$$

where F_d is drag force and δ is boundary layer thickness. The dimensional analysis arguments for obtaining the expression for drag force in Eq. 2.2 are also supported by mathematical arguments (Imai 1957) and related discussion can be found in Ref. (Dyke 1971). The coefficient of drag (C_d^{ic}) from F_d on the original sphere can be expressed as:

$$C_d^{ic} = C_0 \left[1 + \frac{\delta_0}{(Re)^{1/2}}\right]^2 \quad (2.3)$$

where $\delta/R \approx \delta_0/\sqrt{Re}$, the superscript ‘ic’ denotes incompressible regime, and $Re_\infty = \rho_\infty U_\infty D/\mu$ for diameter D of the sphere, and $C_0 \delta_0^2 = 24$, which reduces to Stokes’s result for low Re . Abraham Abraham (1970) found $\delta_0 = 9.06$ based on fitting the correlation to limited experimental data.

Subsonic compressible flow ($M_\infty \leq 1.0$): Compressibility results in density changes, which for $M_\infty < 1.0$ can be accounted by applying a correction to the incompressible formulation. We map the boundary layer of a weakly compressible flow to an equivalent incompressible flow using Howarth (1948) and Stewartson (1949) transformation. The schematic showing the transformation ($U_\infty \rightarrow \tilde{U}, \rho_\infty \rightarrow \tilde{\rho}, T_\infty \rightarrow \tilde{T}$) is presented in Fig. 1(b), and algebraic details are given in the Supplementary Information. Including compressibility effects, the expression for drag coefficient for compressible flow is:

$$C_d^c = C_0 \Theta_\infty \left[1 + \frac{\delta_0}{(\tilde{Re}_\infty)^{1/2}}\right]^2 \quad (2.4)$$

where

$$\Theta(M) = \left(\frac{\tilde{T}}{T}\right)^{\gamma/(\gamma-1)} = \left[1 + (\gamma-1) \frac{M^2}{2}\right]^{\gamma/(\gamma-1)} \quad (2.5)$$

$$\tilde{Re}(Re, M) = Re \Theta(M) \frac{\gamma+1}{2\gamma} - \frac{\gamma-1}{\gamma} \omega \quad (2.6)$$

where \tilde{Re}_∞ and Θ_∞ are respectively equivalent to $\tilde{Re}(\dots)$ and $\Theta(\dots)$ evaluated at free-stream conditions (Re_∞, M_∞), γ is the ratio of specific heat capacities at constant pressure and volume and ω is the exponent in the power-law dependence of viscosity ($\mu \propto T^\omega$) on the temperature. Before we proceed to supersonic flow regime, we point out that accurate prediction in the subsonic regime requires modification of the parameter δ_0 to 9.4 from 9.06. The modified δ_0 does not modify incompressible drag, as shown in Fig. 2, compared to the original value of δ_0 .

Supersonic Flow ($1 \leq M_\infty \leq 5$): When a flow becomes supersonic, a thin region known as a shockwave causes rapid compression of the gas. For normal shocks, an analytical solution can be obtained relating the pre and post-shock states of the gas; these relations are known as Rankine-Hugoniot jump conditions. The post-shock state always corresponds to an increase in temperature, density and pressure, and a decrease in flow field velocity (which is always subsonic). However, for blunt bodies the shock is not normal and curves significantly around the body of interest. This is commonly

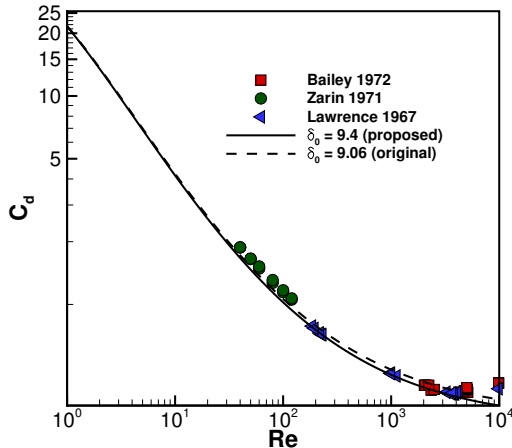


FIGURE 2. Comparison of Eq. 2.3 for drag coefficient in incompressible limit. Experimental data is taken from Refs. (Bailey & Hiatt 1972), (Zarin & Nicholls 1971), and (Goin & Lawrence 1968).

known as a bow shock. Bow shocks are formed around spherical bodies for supersonic and hypersonic flows.

To extend the drag model to supersonic conditions, the same formulation developed in Eqs. 2.4 and 2.6 is employed, with an additional contribution to the drag (Cd_p) due to pressure changes across shock. The effect of compression due to the shock-wave is approximated by using a set of effective flow variables. First, the Rankine-Hugoniot conditions across a normal shock are used to obtain post-shock conditions (given in the Supplementary Information) ($U_\infty \rightarrow U_s, \rho_\infty \rightarrow \rho_s, T_\infty \rightarrow T_s, p_\infty \rightarrow p_s$). To approximate effects of the non-normal (hyperbolic) structure of the shock, we introduce mapping functions $\alpha(M_\infty)$ and $\phi(M_\infty)$ to transform post-shock variables ($U_s \rightarrow \alpha U_s, \rho_s \rightarrow (1/\alpha)\rho_s, T_s \rightarrow \phi T_s, p_s \rightarrow p_s^{\text{ef}}, M_s \rightarrow M_s$) as shown in Fig. 1(c). The inverse scaling (α and $1/\alpha$) for density, and velocity, respectively ensures mass conservation. The function ϕ is obtained by the constraint that the transformation preserves post-shock Mach number (M_s), yielding $\phi = \alpha^2$. Using the transformation of the flow variables, the pressure change term (Cd_p) can be approximated as:

$$Cd_p = C_1 \frac{1}{(1/2)\rho_\infty U_\infty^2} [p_s^{\text{ef}} - p_\infty] \quad (2.7)$$

where p_s^{ef} is the effective pressure and C_1 is the scaling for the contribution of pressure change across a curved shock. The pressure term (Cd_p) does not contain an effective area term, which includes boundary layer thickness, because the pressure does not significantly vary within the boundary layer and therefore is applied directly on the original sphere of radius (R). Expressing the pressure change in terms of the difference in momentum flux between free-stream (at ρ_∞ and U_∞) and the effective momentum flux (at $(1/\alpha)\rho_s$ and αU_s) after the shock-wave, we get

$$Cd_p = \left[C_1 \left(1 - \alpha \frac{U_s}{U_\infty} \right) \right] \quad (2.8)$$

Therefore, the expression for overall drag coefficient becomes:

$$C_d^c = \left[C_1 \left(1 - \alpha \frac{U_s}{U_\infty} \right) \right]^2 + [C_0 \theta_s] \left(1 + \frac{\delta_0}{(\tilde{R}\tilde{e}_s)^{1/2}} \right)^2 \quad (2.9)$$

where the second term in Eq. 2.9 is the same as in Eq. 2.4 but is now evaluated at the effective Mach number, M_s , and \tilde{Re}_s . M_s is invariant under the proposed transformation, and \tilde{Re}_s is given by:

$$\tilde{Re}_s = Re_\infty \left[\frac{1}{\alpha^2} \frac{T_\infty}{T_s} \right]^\omega \Theta_s^{\frac{\gamma+1}{2\gamma} - \frac{\gamma-1}{\gamma}} \omega \quad (2.10)$$

where Θ_s is equivalent to Θ evaluated at effective conditions after transformation. The temperature ratio raised to the power ω appears in Eq. 2.10 due to the ratio of viscosities across the shock. While the estimation of the transport coefficients at high-temperature (Mankodi *et al.* 2020; Oblapenko & Kustova 2020), the power-law with $\omega = 0.74$ is the most widely used relation for viscosity at high temperatures for air (> 600 K). Furthermore, although the Stewartson-Howarth transformation, utilized to derive the function Θ , uses $\omega = 1$ for algebraic simplification, the correlation is not sensitive to the magnitude of ω in the Θ function. The algebraic details for \tilde{Re}_s are provided in the appendix (refer to Sec. A.2). There are two unknown parameters C_1 and α , which are required in Eq. 2.9 to determine C_d . For estimating the expression of α , owing to the difficulty of analytically obtaining a solution, we rely on heuristic arguments. For $M_\infty \gg 1$, for the effective flow to remain continuum ($\tilde{K}n_s < 0.1$, see Eq. 2.1), \tilde{Re}_s should not reduce to zero, implying $\alpha \propto 1/M_\infty$ ($T_\infty/T_s \propto 1/M_\infty^2$ for $M_\infty \gg 1$). A simple formulation for α satisfying this condition (in addition to α being unity for $M_\infty = 1$) is:

$$\alpha = \frac{1}{\alpha_0 M_\infty + 1 - \alpha_0} \quad (2.11)$$

where α_0 is an unknown constant parameter. Recall C_1 is a scaling factor for the pressure term and is obtained from the solution for the hypersonic limit in the next subsection.

Hypersonic Limit ($M_\infty \geq 5$): In hypersonic flow, the post-shock gas is in thermal and chemical nonequilibrium, and the simplified assumption of calorically perfect gas utilized in supersonic flows become inaccurate. In fact, nonequilibrium reaction chemistry modeling, calculation of transport coefficients, and development of appropriate boundary conditions for hypersonic flows are an active area of research. The objective of the present work is to find a scaling of the drag coefficient in the hypersonic regime, an approximation to which has been obtained by Hornung *et al.* (2019) under the assumption of negligible viscous effects. Hornung *et al.* show that the magnitude of the drag coefficient approaches a nearly constant value at high M_∞ , which is also supported by earlier theoretical investigations (Lighthill 1957) and experimental data. In current work, we utilize the hypersonic limit ($C_d^{M_\infty} \approx 0.9$, please refer to Fig. 17 in Ref. (Hornung *et al.* 2019) for more details) to estimate the expression for C_1 in the proposed formulation (Eq. 2.9) for the drag correlation. Substitution of variables (U_s/U_∞ , M_s^2 , Θ , and α) in the limit of $M_\infty \gg 1$ in Eq. 2.9 and equating the corresponding C_d to $C_d^{M_\infty}$ yields the expression for C_1 :

$$C_1 = \frac{C_d^{M_\infty} - C_0 \left[1 + \frac{(\gamma-1)^2}{4\gamma} \right]^{\gamma/(\gamma-1)}}{1 - \frac{1}{\alpha_0} \frac{\gamma-1}{M_\infty \gamma + 1}} \quad (2.12)$$

For more algebraic details or the exact high Mach number limit of the variables, please refer to Sec. A.3 of the appendix. At this stage our continuum formulation for the expression of the drag coefficient is complete (Eq. 2.9), with only one unknown parameter

α_0 . Before, we estimate α_0 , the extension of the model to rarefied regime is presented next.

2.2. Theoretical Development: Rarefaction Regime

In rarefied flows ($Kn_\infty > 0.01$), due to fewer gas molecule collisions near the surface, the bulk velocity and temperature of the gas do not equilibrate with the surface velocity and surface temperature, respectively. This results in a finite velocity slip and temperature jump at the wall. To account for these non-continuum effects, velocity slip (and temperature jump) at the wall is employed along with the Navier-Stokes equations. At higher Kn_∞ (> 0.5), the stress tensor (and heat flux vector) does not depend linearly on the velocity gradient (and temperature gradient); therefore, the Navier-Stokes equations become inaccurate in high Kn_∞ regimes. If M_∞ is also high, as molecules travel larger distances without collisions at high Kn_∞ , the shock-layer and boundary layer merge with each other. Although the Boltzmann equation is applicable for arbitrary degree of rarefaction ($\forall Kn_\infty$), the equation is computationally expensive to solve. However, approximate scaling laws relevant to drag correlation can still be informed from the Boltzmann equation, which is adequate for the current work and is described in the next subsections.

Rarefaction correction ($\forall Kn_\infty$) at low M_∞ : For low speed flows, the Boltzmann equation has been theoretically solved in an approximate manner by Phillips (1975) for estimating the drag force on a sphere. Phillips expressed $C_d = f_{Kn} C_d^c$, where f_{Kn} is a multiplicative rarefaction correction to the continuum drag coefficient (C_d^c). For low speed flows, numerically identical to the expression by Phillips (Phillips 1975), an alternate simple closed form expression for f_{Kn} has been proposed (Clift *et al.* 1978) (and for non-spherical particles in Ref. (Dahneke 1973)) as follows:

$$f_{Kn} = \frac{1}{1 + Kn_\infty [A_1 + A_2 \exp[-A_3/Kn_\infty]]} \quad (2.13)$$

where $A_1 = 2.514$, $A_2 = 0.8$, and $A_3 = 0.55$. The correction in Eq. 2.13 was earlier proposed by Millikan (1923) and is valid for all Knudsen numbers (Clift *et al.* 1978) for low M numbers. Basically, f_{Kn} reduces to the high-Kn number drag expression for high Kn ($\gg 1$) and unity at low Kn_∞ (< 0.01). An intuitive argument for the justification of Eq. 2.13 using a reduced sphere due to slip effects is presented in the appendix (Sec. A.4). Next, we develop the correction function for high Kn_∞ and high M_∞ .

Rarefaction correction for the slip ($0.01 \leq Kn_\infty < 0.1$) and transition ($0.1 \leq Kn_\infty < 10$) regime at high M_∞ : For high Mach number flows ($M_\infty > 0.3$) flows, an analytical solution of the Boltzmann equation is challenging, and in many cases, impossible. Several sets of non-linear constitutive relations and higher order moment equations have been proposed (Singh & Agrawal 2016; Singh *et al.* 2017; Struchtrup 2005) as computationally efficient alternatives to the Boltzmann equation for modeling slip and transition regimes. For high-speed flow over a sphere, Singh and Schwartzentruber (Singh & Schwartzentruber 2016, 2017) mathematically showed that the ratio of the non-linear to linear (used in the Navier-Stokes equations) constitutive relations dominantly depends on a non-dimensional number called W_r^T , which is given by:

$$W_r^T = W_r \left(1 + \frac{T_p}{T_s} \right)^\omega \quad M_\infty > 1 \quad (2.14)$$

where

$$W_r = \frac{M_\infty^{2\omega}}{Re_\infty} = Kn_\infty M_\infty^{2\omega-1} \sqrt{\frac{2}{\pi\gamma}} \quad (2.15)$$

and T_p is surface temperature. In fact, an approximate contribution of the higher order (up to infinite order in terms of Kn_∞) constitutive relations has been shown as a scaling factor to the heat transfer coefficient. At high Kn_∞ , the gas does not fully thermally accommodate with the wall, and the drag force depends explicitly on the surface temperature as also evident in Eq. 2.14. We employ the same correction to f_{Kn} , which modifies the high Knudsen number correction using an additional term based on W_r :

$$f_{Kn,W_r} = \frac{1}{1 + Kn_\infty [A_1 + A_2 \exp(-A_3/Kn_\infty)]} \frac{1}{1 + \alpha_{hoc} W_r^T} \quad (2.16)$$

Equation 2.16 corrects the drag coefficient for rarefaction effects at moderate Kn_∞ and at high M_∞ .

Rarefaction correction for free-molecular regime ($Kn_\infty \geq 10$) at high M_∞ :
As a final step, we bridge the correlation to the analytically obtained C_d for the free-molecular regime. An analytical expression for C_d valid for free-molecular flow has been developed by (Patterson 1971) and is given by:

$$Cd_{fm} = \frac{(1 + 2s^2)\exp(-s^2)}{s^3\sqrt{\pi}} + \frac{(4s^4 + 4s^2 - 1)\text{erf}(s)}{2s^4} + \frac{2}{3s}\sqrt{\pi}\frac{T_p}{T_\infty} \quad (2.17)$$

where $s = M_\infty\sqrt{\gamma/2}$. Singh & Schwartzentruber (2017) proposed a bridging function between a purely empirical drag correlation for high $M(> 1)$ transition and free-molecular regimes using the inverse Cheng's parameter (Cheng 1961), K_c . Mathematically, $1/K_c^2 \propto \mu^*T_\infty/\mu_\infty T^*$, where T^* is the average of T_s and T_p and μ^* is evaluated at T^* . Substituting power-law relations for viscosity, it can be shown that the inverse of K_c is proportional to W_r^T , both of which depend on the wall temperature that becomes important as the degree of rarefaction increases. In this work, we employ $Br(\propto W_r^T)$ as the correlation parameter to bridge the proposed general physics-based drag correlation to the free-molecular expression,

$$Br = W_r^T \frac{M_\infty^{2\omega-1} + 1}{M_\infty^{2\omega-1}} \quad (2.18)$$

Br has the desirable properties that for $M_\infty \gg 1 \implies Br \rightarrow W_r^T$ and for $M_\infty \ll 1 \implies Br \rightarrow Kn_\infty$. Using a rational polynomial function as a plausible bridging function, the expression for full drag correlation is defined as:

$$C_d = C_d^c(M, Re) f_{Kn,W_r} \frac{1}{1 + Br^\eta} + Cd_{fm} \frac{Br^\eta}{1 + Br^\eta} \quad (2.19)$$

where η is an unknown parameter. Equation 2.19 is the main result of the present work. There are three unknown parameters α_0, α_{hoc} and η , which are obtained in the next subsection. The complete set of equations, for the entire correlation, are also provided separately in Sec. C of the appendix.

2.3. Estimation of α_0 , α_{hoc} , and η

Least-square fitting was used to determine the unknown parameters based on available experimental data and relevant simulations. A summary of the data used for fitting

Parameters	Physical Significance	Magnitude
δ_0	boundary layer thickness scaling	9.4
α_0	shock-curvature parameter	0.356
A_1, A_2, A_3	low-speed rarefaction correction (Clift <i>et al.</i> 1978)	2.514, 0.8, 0.55
η	bridging function modulator	1.8
α_{hoc}	high speed rarefaction correction	1.27

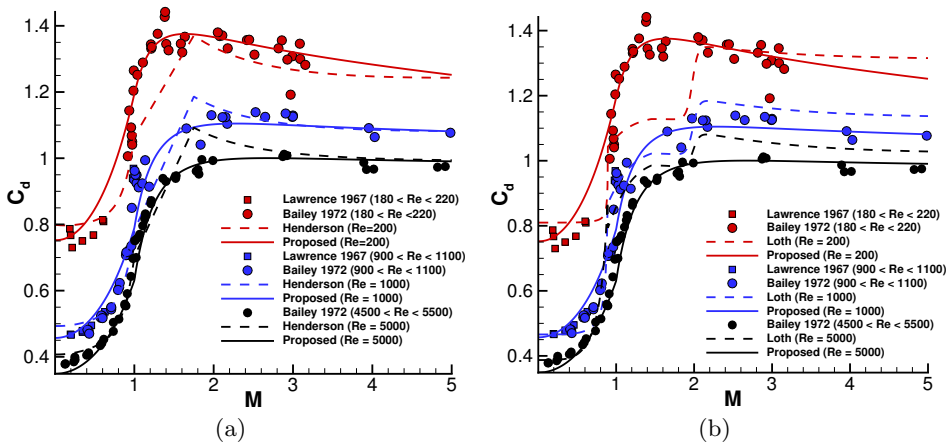


FIGURE 3. Comparison of the proposed model with experimental data, Loth model, and Henderson model

unknown parameters is compiled in this section. Bailey & Hiatt (1972) determined drag on spherical bodies for a wide range of Mach and Reynolds numbers ($0.1 < M_\infty < 6$ and $10^1 < Re_\infty < 10^5$) in a ballistic range. Bailey (1966) also determined the drag on spheres for higher Reynolds numbers using a similar setup. Sreekanth (1962) determined the drag on spherical bodies in the transitional Knudsen number regime ($M_\infty = 2$ and $0.1 < Kn_\infty < 0.8$) using a wind tunnel setup. Zarin & Nicholls (1971) determined the drag on spherical bodies in a subsonic wind tunnel using magnetic suspension for a range of Reynolds numbers ($0.1 < M_\infty < 0.57$ and $4 \times 10^1 < Re_\infty < 5 \times 10^4$). used CFD and DSMC, respectively, to determine the drag on a spherical body Kissel (2003); Overell (2003); Macrossan (2006). Aroesty measured spherical drag in Berkeley's low-density wind tunnel for Mach numbers of roughly 2, 4 and 6 for $10^1 < Re_\infty < 10^4$ Aroesty (1963). Goin & Lawrence (1968) used a ballistic range to determine drag for subsonic spheres ($0.1 < M_\infty < 1$) for a range of Reynolds numbers ($2 \times 10^1 < Re_\infty < 10^4$). Charters & Thomas (1945) also used a ballistic range setup and determined drag on spheres for a larger range of Mach numbers at relatively high Reynolds numbers ($0.3 < M_\infty < 4$ and $9.3 \times 10^4 < Re_\infty < 1.3 \times 10^6$). Hodges (1957) determined drag on supersonic and hypersonic spheres ($2 < M_\infty < 10$) for very high Reynolds numbers ($Re_\infty > 3 \times 10^6$). May also found the drag on spherical bodies, but for lower Reynolds numbers and Mach numbers ($0.8 < M_\infty < 4.7$ and $1.1 \times 10^3 < Re_\infty < 8.4 \times 10^5$). The obtained parameters from least-square fitting are listed in Table 1.

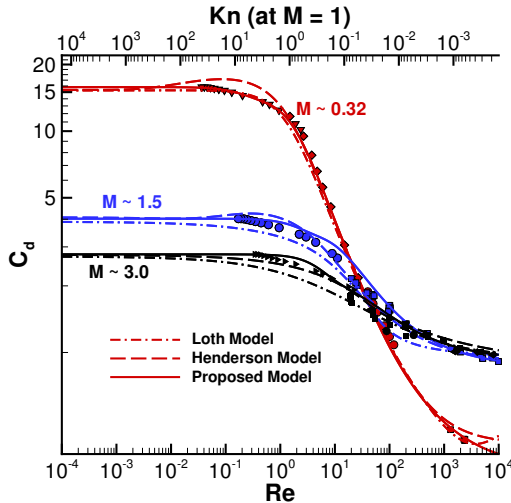


FIGURE 4. Comparison of the proposed model, Hendersons model, Loths model, and experimental data vs Re for $M = 0.32, 1.5$ and 3.0 in red, blue, and black color respectively. Experimental data is taken from several sources: the red circular symbols from Ref. (Zarin & Nicholls 1971), red squares from Ref. (Goin & Lawrence 1968), blue and black squares from Ref. (Bailey & Hiatt 1972), and black diamonds from Ref. (May & WITT 1953). The red triangles, red diamonds, blue circles, and black triangles correspond to the DSMC data taken from Ref. (Li *et al.* 2019). The top axis denotes Knudsen numbers, evaluated at $M_\infty = 1$ using Eq. 2.1.

3. Results and Discussion

In this section, we compare the proposed drag model with state-of-the-art models. We then present the drag correlation results for different species type (monatomic, diatomic, and triatomic gases). Lastly, we apply the proposed model to investigate sensitivity to surface heating rates for dusty flow over a sphere, relevant for high-speed flows in Mars atmosphere.

3.1. Comparison to State-of-the-art Models

We compare the proposed model to standard empirical models that are widely used in the literature. Specifically, the results are compared with Henderson (1976) and Loth (2008) models. The equations for both models are reported in in Sec. B of the appendix.

In Figure 3(a), the proposed model is compared with Henderson model and experimental data with Mach numbers for a range of Re corresponding to the continuum regime. For subsonic and hypersonic regimes, both the Henderson and proposed models fit the data adequately. However, near the transonic and supersonic regimes, the proposed model predicts the experimental data more accurately than the Henderson model. This is not surprising; the Henderson model interpolates the drag in these regimes ($1 \geq M_\infty \geq 1.75$), while the proposed model has systematically incorporated shock-wave physics. Next, we compare the proposed model with the Loth model.

Figure 3(b) compares the proposed model with the experimental data and the Loth model for a wide range of Re_∞ as a function of M_∞ in the continuum regime. While the Loth model predicts the subsonic regime data as accurately as the proposed model, the disagreement at high M_∞ numbers is significant, specifically near transonic and supersonic regimes. The Loth model is based on fitting the data such that C_d remains invariant if M_∞ is varied but Re is kept fixed at 45. The proposed model does significantly

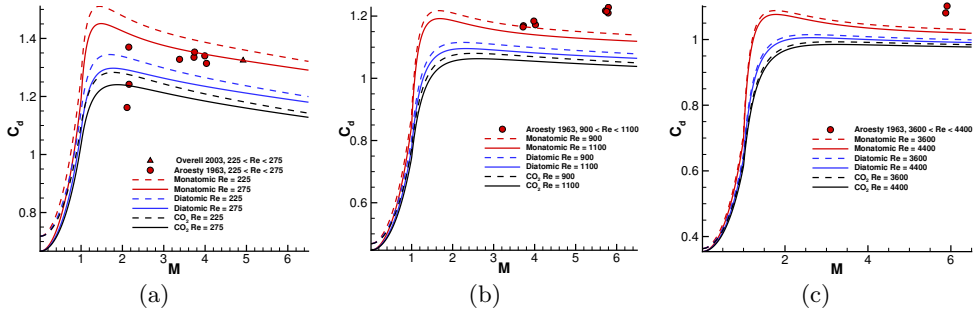


FIGURE 5. Comparison of the proposed model using different gas types. Experimental data from Aroesty and CFD simulations from Overell are also included, both of which considered monatomic gases.

better compared to the Loth model at all M_∞ . In terms of the entire data considered, the relative L_2 norm of the errors of the proposed correlation, Henderson model and Loth model, when compared to the experimental data are 7.6, 15.8 and 12.1 respectively.

Next, we compare the proposed model, Henderson model, and Loth model for a range of Re_∞ in Fig. 4, which includes data from continuum to free-molecular regime for three different free-stream M_∞ . All three models compare reasonably well with the data with discrepancies in certain regimes. Firstly, the proposed model predicts accurate drag coefficients in the free-molecular (low Re) limit for subsonic data supported by the DSMC data at these conditions. However, in the limit of very high Kn , the Knudsen number correction from Eq. 2.13 scales correctly compared to the free-molecular limit, but differs by a constant factor. Loth’s model approaches this limit as opposed to the free-molecular limit, which is the reason for the discrepancy for the subsonic data. While the proposed model agrees well with the experimental data, it deviates slightly in the transitional regime. The proposed model under and over-predicts over short a range of Re . It is noted that the bridging function is semi-empirical and is based on non-linear constitutive relations scaling and data fitting. Additional data could help improve the parameterization of this transition region. For instance, the proposed correlation can be used as an input feature for a neural-network approach in the transition regime, and the fidelity could be improved (Li *et al.* 2019).

3.2. Sensitivity of the drag correlation to γ (the ratio of specific heat capacities)

We proceed by examining effects of thermodynamic properties of the gas on the drag coefficient. This subsection demonstrates that since the proposed model is physics-based, the model embeds explicit dependence on the gas-specific properties. For instance, the proposed drag model explicitly depends on the ratio of specific heat capacities at constant pressure and volume, which is different for monatomic, diatomic, and triatomic gas. In Fig. 5, the proposed correlation is plotted against M for three different Re ranges, for monatomic, diatomic, and triatomic linear molecules (CO_2 in the present work). Firstly, the drag coefficient is higher for monatomic gas than triatomic gas. This difference is only significant at high $M_\infty \geq 1$. Since monatomic gas have higher γ compared to triatomic gas, they have fewer energy modes for thermal energy re-distribution generated due to the conversion of bulk energy across a shockwave. Therefore, the resulting higher post-shock pressure and velocity for monatomic gases (please refer to Eqs. A 5 and A 4) results in higher drag coefficient. The experimental data from Aroesty (1963) corresponds to monatomic gas (argon), and therefore provides a test-bed to investigate the sensitivity

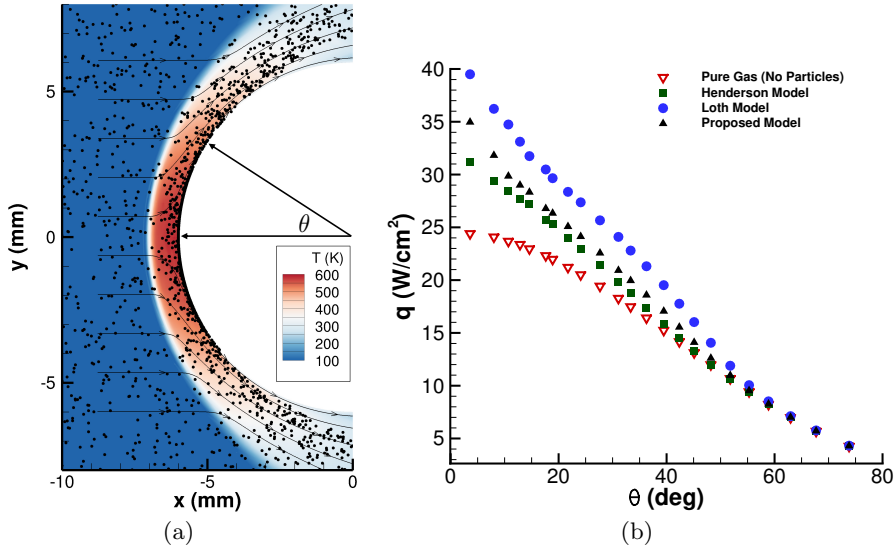


FIGURE 6. Pure-gas and dusty-gas surface heat flux profiles for a flow over a sphere of diameter 0.012 m and surface temperature of 300 K. The free-stream conditions are characterized by $Ma_\infty = 6.1$, and $P_\infty = 1000$ Pa, $T_\infty = 68$ K. The dust particles are made of SiO_2 , with a density of 2264 kg/m^3 , mean diameter of $0.19 \mu\text{m}$ and 3% mass loading ratio (the mass loading ratio is the ratio of the mass flux of the particles to the mass flux of the gas).

of the drag to γ . Figure 5(a) shows that the proposed correlation for monatomic gas is in reasonably good agreement with experimental data. Alternatively, changing gas-type from triatomic (CO_2) to a monatomic gas shifts the predictions from the correlation in the direction of experimental data, for all three ranges of Re considered.

3.3. Sensitivity of the drag correlation to surface heat flux for a high-speed dusty gas flow over a sphere

In this subsection, the proposed correlation is applied to model trajectories of dust particles in a high-speed flow over a sphere. Understanding high-speed particle-laden flows is relevant for entry to Mars atmosphere, where dust storms are frequent (Fernández 1997) and is also relevant for hypersonic flight within Earth’s atmosphere, where particulates, droplets, or ice-crystals may be present. Recently, Ching *et al.* (2020) simulated high-speed nitrogen flow seeded with dust particles over a sphere, showing that surface heat flux is amplified by the presence of the dust particles due to interphase momentum transfer and inelastic particle-wall collisions. Interestingly, the extent of the amplification of surface heat flux was found to be sensitive to the employed drag correlations. In addition to the drag correlation, the accuracy of the surface heat flux depends on several factors, such as the employed heat flux correlation (Fox *et al.* 1978), and other physical mechanisms, the details of which can be found in Ref. (Ching *et al.* 2020). In this work, we perform sensitivity analysis focusing on the drag correlation, and therefore apply the proposed drag correlation to the same flow configuration considered in Ref. (Ching *et al.* 2020) and compare the surface heat flux obtained with other drag models. Third-order backwards difference and the third-order Adams-Bashforth method are employed to integrate the gas and particles in time, respectively. A third-order discontinuous Galerkin (DG) schemes have been shown to have robust heat transfer predictive capability (Ching *et al.* 2019b). To simulate dust particles suspended in the carrier gas, a Lagrangian

particle method under the DG framework (Ching *et al.* 2019a) has been employed. At each time step, particles are injected at random locations along the inflow boundary. Further simulation details can be found in Ref. (Ching *et al.* 2020).

Figure 6(a) shows the temperature contour and the distribution of dust particles for a high speed nitrogen gas flow over a sphere. In Figure 6(b), the surface heat flux distribution obtained with the proposed drag correlation, is compared to that obtained using the Henderson and Loth models for trajectory estimation. Simulations with pure gas (i.e. no dust particles) show lower surface heat flux relative to the dusty gas. Using the proposed correlation, the heat flux predictions deviate by nearly $\pm 14\%$ from the Henderson (+) and Loth (-) models.

4. Conclusions

We develop a general drag coefficient model for spherical particles moving in a fluid, applicable for arbitrary particle relative velocity, particle diameter, gas pressure, gas temperature, and surface temperature. In addition to free-stream Mach number (M_∞) and Reynolds number (Re_∞), the proposed drag model encapsulates explicit dependence on the particle's surface temperature, the ratio of specific heat capacities (γ), a non continuum parameter ($W_r \propto M_\infty^{2\omega}/Re_\infty$), and the power-law index (ω) of viscosity ($\mu \propto T^\omega$). The correlation reproduces known theoretical results in limiting situations. The correlation is formulated by incorporating simple physics-based scaling laws to model low-speed hydrodynamics, high-speed shock-wave physics and non continuum effects due to rarefied gas dynamics. Free-parameters introduced in the scaling laws are obtained by using experimental data for drag coefficients from the literature. The proposed correlation is demonstrated to be in better agreement with the experimental data compared to widely used drag models.

The dependence of the drag model on γ , and therefore on the gas-composition is investigated. The distinct trend of higher drag coefficients for monatomic gas compared to diatomic gas in experimental measurements is captured quantitatively by the proposed drag model.

Finally, the proposed drag model is applied to evaluate trajectories of particles in a simulation of high-speed dusty flow over a sphere. Enhancement of the surface heat transfer coefficient due to particle-flow and particle-surface interactions is found to be significantly different when using the new correlation compared to state-of-the-art empirical drag models.

Declaration of Interests

Declaration of Interests. The authors report no conflict of interest.

Acknowledgments

This work is supported by ONR FY2020 MURI grant N00014-20-1-2682, NASA NSTRF grant 80NSSC19K1129, and NASA Early Career Faculty grant (NNX15AU58G) from the NASA Space Technology Research Grants Program.

Appendix A. Mathematical details related to the transformations used in derivation of the drag model

In this section, we provide additional algebraic details required in the derivation of the proposed drag model.

A.1. Mapping weakly compressible boundary layer to incompressible boundary layer variables

Howarth (1948) and Stewartson (1949) introduced transformation to map a compressible laminar boundary layer to an equivalent incompressible boundary layer. The required transformed variables, denoted by $\tilde{\cdot}$, in terms of free-stream variables can be expressed as:

$$\frac{\tilde{T}}{T_\infty} = 1 + (\gamma - 1) \frac{M_\infty^2}{2}; \quad \frac{\tilde{\rho}}{\rho_\infty} = \left(\frac{\tilde{T}}{T_\infty} \right)^{1/(\gamma-1)} \quad (\text{A } 1)$$

Using the transformed variables along with mass conservation ($\rho_\infty U_\infty = \tilde{\rho}_\infty \tilde{U}_\infty$), Re_∞ can be transformed to \tilde{Re} :

$$\tilde{Re}(M_\infty, Re_\infty) = Re_\infty \left(\frac{\tilde{T}}{T} \right)^{\frac{2-\gamma}{\gamma-1}} \frac{\tilde{T} + S}{\tilde{T} + S} \quad (\text{A } 2)$$

where S is the parameter in the Sutherland law of viscosity.

A.2. Transformation of variables across a shock-wave in the supersonic regime

Post-shock conditions across a normal shock can be obtained via Rankine-Hugoniot Rankine (1870); Hugoniot (1887) conditions which are:

$$\frac{T_s}{T_\infty} = \frac{[(\gamma - 1)M_\infty^2 + 2][2\gamma M_\infty^2 - (\gamma - 1)]}{(\gamma + 1)^2 M_\infty^2} \quad (\text{A } 3)$$

$$\frac{p_s}{p_\infty} = \frac{2\gamma}{\gamma + 1} M_\infty^2 - \frac{\gamma - 1}{\gamma + 1} \quad (\text{A } 4)$$

$$\frac{u_s}{u_\infty} = \frac{2 + (\gamma - 1)M_\infty^2}{(\gamma + 1)M_\infty^2} \quad (\text{A } 5)$$

Using the jump conditions, post-shock M_s can be written as:

$$M_s = \sqrt{\frac{(\gamma - 1)M_\infty^2 + 2}{2\gamma M_\infty^2 - (\gamma - 1)}} \quad (\text{A } 6)$$

To obtain Reynolds number (\tilde{Re}_s), the post-shock Reynolds number (Re_s) is first obtained using the Rankine-Hugoniot conditions, and then transformed using the proposed transformation for curvature effects to obtain Re_s^{ef} .

$$Re_s^{\text{ef}} = Re_\infty \left(\frac{T_\infty}{\alpha^2 T_s} \right)^\omega \quad (\text{A } 7)$$

The second step is to employ the Stewartson-Howarth transformation for weak compressibility effects corresponding to the post-shock Mach number (M_s) using Eq. 2.6:

$$\begin{aligned} Re_s &= Re_s^{\text{ef}} \Theta(M) \frac{\gamma + 1}{2\gamma} - \frac{\gamma - 1}{\gamma} \omega \\ &= Re_\infty \left(\frac{T_\infty}{\alpha^2 T_s} \right)^\omega \end{aligned} \quad (\text{A } 8)$$

A.3. Drag coefficient in the hypersonic limit

The additional variables (U_s/U_∞ , M_s^2 , Θ , and α) in the limit of $M_\infty \gg 1$ required in Eq. 2.9 to estimate C_1 are

$$\frac{U_s}{U_\infty} \Big|_{M_\infty \gg 1} = \frac{\gamma - 1}{\gamma + 1} \quad (\text{A } 9)$$

$$M_s^2 \Big|_{M_\infty \gg 1} = \frac{\gamma - 1}{2\gamma} \quad (\text{A } 10)$$

$$\Theta \Big|_{M_\infty \gg 1} = \left[1 + (\gamma - 1) \frac{M_s^2}{2} \right]^{\gamma/(\gamma-1)} = \left[1 + \frac{(\gamma - 1)^2}{4\gamma} \right]^{\gamma/(\gamma-1)} \quad (\text{A } 11)$$

$$\alpha \Big|_{M_\infty \gg 1} = \frac{1}{\alpha_0 M_\infty} \quad (\text{A } 12)$$

Employing variables from Eq. A 9 to A 12 in the expression for C_d in Eq. 2.9 yields:

$$\begin{aligned} C_d^c(M_s, Re_s) \Big|_{M_\infty \gg 1} &\rightarrow C_1 \left(1 - \alpha_\infty \frac{\gamma - 1}{\gamma + 1} \right) \\ &+ A_o \left[1 + \frac{(\gamma - 1)^2}{4\gamma} \right]^{\gamma/(\gamma-1)} = C_d^{M_\infty} \\ \Rightarrow C_1 &= \frac{C_d^{M_\infty} - C_o \left[1 + \frac{(\gamma - 1)^2}{4\gamma} \right]^{\gamma/(\gamma-1)}}{1 - \frac{1}{\alpha_0} \frac{\gamma - 1}{M_\infty \gamma + 1}} \end{aligned} \quad (\text{A } 13)$$

A.4. Slip effects and their relevance to drag

In view of our approach (shown in Fig. 1(d)), we present an intuitive argument supporting Eq. 2.13 in the slip flow regime. The effect of velocity slip at the wall can be understood by considering a sphere of smaller radius which has no slip at the wall. The drag coefficient (C_{d_s}) for a sphere with slip boundary condition can be obtained using the drag on the sphere of smaller radius with no slip:

$$C_{d_s} = C_d \left(1 - \frac{\delta_{Kn}}{R} \right)^2 \quad (\text{A } 14)$$

where the δ_{Kn} is the Knudsen layer thickness. A simple scaling for δ_{Kn} based on a stationary wall in terms of slip velocity (u_s) and velocity gradient at the wall ($(\partial u / \partial y)|_w$) can be expressed as $\delta_{Kn} = (u_s) / (\partial u / \partial y)$. Here, u_s is the slip velocity and the wall is assumed stationary. The approximation to u_s using Maxwell's slip model in terms of slip

coefficient (C_{Kn}) and the mean free-path (λ) is given by:

$$u_s = C_{Kn} \lambda \frac{\partial u}{\partial y} \Big|_w \quad (\text{A } 15)$$

Eqs. A 14 and A 15 can be combined to yield an approximate expression for δ_{Kn} as:

$$\frac{\delta_{Kn}}{R} = C_{Kn} Kn \quad (\text{A } 16)$$

Substituting the above expression for δ_{Kn} from Eq. A 16 in Eq. A 14, C_d reduces to:

$$C_d = C_d (1 - C_{Kn} Kn)^2 \quad (\text{A } 17)$$

This Knudsen correction in the limit of small Knudsen number reduces to:

$$C_d \approx C_d (1 - 2C_{Kn} Kn) \quad (\text{A } 18)$$

The expression for C_d in Eq. A 18 is identical to the result obtained theoretically by Basset Basset & Strutt (1888).

Appendix B. Expressions for the Henderson and Loth models

Henderson model:

$$\begin{aligned} C_d(M_\infty, Re_\infty, T_w/T_\infty) &= 24 \left[Re_\infty + s \left\{ 4.33 + \left(\frac{3.65 - 1.53T_w/T_\infty}{1 + 0.353T_w/T_\infty} \right) \exp \left(-0.247 \frac{Re_\infty}{s} \right) \right\} \right]^{-1} \\ &+ \exp \left(-\frac{0.5M_\infty}{\sqrt{Re_\infty}} \right) \left[\frac{4.5 + 0.38(0.03Re_\infty + 0.48\sqrt{Re_\infty})}{1 + 0.03Re_\infty + 0.48\sqrt{Re_\infty}} + 0.1M_\infty^2 \right. \\ &+ 0.2M_\infty^8 \left. \right] + \left[1 - \exp \left(-\frac{M_\infty}{Re_\infty} \right) \right] 0.6s \\ & \hspace{15em} M_\infty < 1 \\ &= \frac{0.9 + \frac{0.34}{M_\infty^2} + 1.86 \left(\frac{M_\infty}{Re_\infty} \right)^{1/2} \left[2 + \frac{2}{s} + \frac{1.058}{s} \left(\frac{T_w}{T_\infty} \right)^{1/2} - \frac{1}{s^4} \right]}{1 + 1.86 \left(\frac{M_\infty}{Re_\infty} \right)^{1/2}} \\ & \hspace{15em} M_\infty > 1.75 \\ &= C_d(1, Re_\infty) + \frac{4}{3}(M_\infty - 1) [C_d(1.75, Re_\infty) - C_d(1, Re_\infty)] \\ & \hspace{15em} 1 \geq M_\infty \geq 1.75 \\ & \hspace{15em} (\text{B } 1) \end{aligned}$$

Loth model:

$$C_d = \frac{24}{Re_\infty} [1 + 0.15Re_\infty^{0.687}] H_M + \frac{0.42C_M}{1 + \frac{42500G_M}{Re_\infty^{1.16}}} \quad Re_\infty > 45 \quad (\text{B } 2)$$

$$C_M = \frac{5}{3} + \frac{2}{3} \tanh [3 \ln (M_\infty + 1)] \quad M_\infty \leq 1.45 \quad (\text{B3})$$

$$C_M = 2.044 + 0.2 \exp \left[-1.8 \ln (M_\infty / 1.5)^2 \right] \quad M_\infty \geq 1.45$$

$$G_M = 1 - 1.525 M_\infty^4 \quad M_\infty < 0.89 \quad (\text{B4})$$

$$G_M = 0.0002 + 0.0008 \tanh [12.77 (M_\infty - 2.02)] \quad M_\infty \geq 0.89$$

$$H_M = 1 - \frac{0.258 C_M}{1 + 514 G_M} \quad (\text{B5})$$

$$C_d = \frac{C_{d,Kn,Re}}{1 + M_\infty^4} + \frac{M_\infty^4 C_{d,fm,Re}}{1 + M_\infty^4} \quad Re_\infty \leq 45 \quad (\text{B6})$$

$$C_{d,Kn,Re} = \frac{24}{Re_\infty} (1 + 0.15 Re_\infty^{0.687}) f_{Kn} \quad (\text{B7})$$

$$f_{Kn} = \frac{1}{1 + Kn_\infty [2.514 + 0.8 \exp(-0.55 / Kn_\infty)]} \quad (\text{B8})$$

$$C_{d,fm,Re} = \frac{C_{d,fm}}{1 + \left(\frac{C'_{d,fm}}{1.63} - 1 \right) \sqrt{\frac{Re_\infty}{45}}} \quad (\text{B9})$$

$$C'_{d,fm} = \frac{(1 + 2s^2) \exp(-s^2)}{s^3 \sqrt{\pi}} + \frac{(4s^4 + 4s^2 - 1) \operatorname{erf}(s)}{2s^4} \quad (\text{B10})$$

$$C_{d,fm} = \frac{(1 + 2s^2) \exp(-s^2)}{s^3 \sqrt{\pi}} + \frac{(4s^4 + 4s^2 - 1) \operatorname{erf}(s)}{2s^4} + \frac{2}{3s} \sqrt{\pi \frac{T_p}{T_\infty}} \quad (\text{B11})$$

Appendix C. Complete equations for the proposed drag model

In this section, we summarize the full set of mathematical expressions required to calculate the drag coefficient.

$$C_d = C_d^c(M_\infty, Re_\infty) f_{Kn_\infty, W_r} \frac{1}{1 + Br^\eta} + C_{d,fm} \frac{Br^\eta}{1 + Br^\eta} \quad (\text{C1})$$

$$Br = W_r^T \frac{M_\infty^{2\omega-1} + 1}{M_\infty^{2\omega-1}} \quad (\text{C2})$$

$$W_r^T = W_r \left(1 + \frac{T_p}{T_s} \right)^\omega \quad M_\infty > 1 \quad (\text{C3})$$

where

$$W_r = \frac{M_\infty^{2\omega}}{Re_\infty} = Kn_\infty M_\infty^{2\omega-1} \sqrt{\frac{2}{\pi \gamma}} \quad (\text{C4})$$

$$f_{Kn_\infty, W_r} = \frac{1}{1 + Kn_\infty [A_1 + A_2 \exp(-A_3 / Kn_\infty)]} \frac{1}{1 + \alpha_{hoc} W_r^T} \quad (\text{C5})$$

$$C_{d,fm} = \frac{(1 + 2s^2) \exp(-s^2)}{s^3 \sqrt{\pi}} + \frac{(4s^4 + 4s^2 - 1) \operatorname{erf}(s)}{2s^4} + \frac{2}{3s} \sqrt{\pi \frac{T_p}{T_\infty}} \quad (\text{C6})$$

$$s = M_\infty \sqrt{\frac{\gamma}{2}} \quad (\text{C7})$$

$$C_d^c = \left[C_1 \left(1 - \alpha \frac{U_s}{U_\infty} \right) \right] + [C_0 \Theta(M_s)] \left(1 + \frac{\delta_0}{(\tilde{Re}_s)^{1/2}} \right)^2 \quad (\text{C8})$$

$$\Theta(M) = \left[1 + (\gamma - 1) \frac{M^2}{2} \right]^{\gamma/(\gamma-1)} \quad (\text{C9})$$

$$\tilde{Re}_s = Re_\infty \left[\frac{1}{\alpha^2} \frac{T_\infty}{T_s} \right]^\omega \Theta(M) \frac{\gamma + 1}{2\gamma} - \frac{\gamma - 1}{\gamma} \omega \quad (\text{C10})$$

$$C_1 = \frac{C_d^{M_\infty} - A_o \left[1 + \frac{(\gamma - 1)^2}{4\gamma} \right]^{\gamma/(\gamma-1)}}{1 - \frac{1}{\alpha_0 M_\infty} \frac{\gamma - 1}{\gamma + 1}} \quad (\text{C11})$$

$$\alpha = \frac{1}{\alpha_0 M_\infty + 1 - \alpha_0} \quad (\text{C12})$$

REFERENCES

- ABRAHAM, FARID F 1970 Functional dependence of drag coefficient of a sphere on Reynolds number. *The Physics of Fluids* **13** (8), 2194–2195.
- AKEDO, JUN 2006 Aerosol deposition of ceramic thick films at room temperature: Densification mechanism of ceramic layers. *Journal of the American Ceramic Society* **89** (6), 1834–1839.
- AROESTY, JEROME 1963 Sphere drag in a low-density supersonic flow. In *Rarefied Gas Dynamics*, vol. 2, p. 261.
- BAILEY, A. 1966 Sphere drag measurements in an aeroballistics range at high velocities and low Reynolds numbers.
- BAILEY, A. B. & HIATT, J. 1972 Sphere drag coefficients for a broad range of Mach and Reynolds numbers. *AIAA Journal* **10** (11), 1436–1440.
- BASSET, ALFRED BARNARD & STRUTT, JOHN WILLIAM 1888 On the motion of a sphere in a viscous liquid. *Philosophical Transactions of the Royal Society of London* **179**, 43–63.
- CHARTERS, A. C. & THOMAS, R. N. 1945 The aerodynamic performance of small spheres from subsonic to high supersonic velocities. *Journal of the Aeronautical Sciences* **12** (4), 468–476.
- CHENG, HSIEN KEI 1961 *Hypersonic shock-layer theory of the stagnation region at low Reynolds number*. Cornell Aeronautical Laboratory.
- CHING, E. J., BARNHARDT, M. D. & IHME, M. 2020 Sensitivity of hypersonic dusty flows to physical modeling of the particle phase. Submitted to *Journal of Spacecraft and Rockets*.
- CHING, E. J., BRILL, S. R., LV, Y., BARNHARDT, M. D. & IHME, M. 2019a An Euler-Lagrange method for simulating high-speed multiphase flows with two-way-coupling using discontinuous Galerkin schemes on arbitrary curved elements. *Journal of Computational Physics* Under review.
- CHING, ERIC J, LV, YU, GNOFFO, PETER, BARNHARDT, MICHAEL & IHME, MATTHIAS 2019b Shock capturing for discontinuous Galerkin methods with application to predicting heat transfer in hypersonic flows. *Journal of Computational Physics* **376**, 54–75.
- CLIFT, R., GRACE, J.R & WEBER, M.E. 1978 *Bubbles, Drops and Particles*. Dover Civil and Mechanical Engineering.

- DAHNEKE, BARTON E 1973 Slip correction factors for nonspherical bodies—III the form of the general law. *Journal of Aerosol Science* **4** (2), 163–170.
- DYKE, MILTON VAN 1971 Comments on “functional dependence of drag coefficient of a sphere on Reynolds number”. *The Physics of Fluids* **14** (5), 1038–1039.
- FERNÁNDEZ, WALTER 1997 Martian dust storms: A review. *Earth, Moon, and Planets* **77**, 19–46.
- FOX, T. W., RACKETT, C. W. & NICHOLLS, J. A. 1978 Shock wave ignition of magnesium powders. In *11th International Shock Tubes and Waves Symposium*, pp. 262–268. Seattle, Washington.
- GOIN, K. L. & LAWRENCE, W. R. 1968 Subsonic drag of spheres at Reynolds numbers from 200 to 10,000. *AIAA Journal* **6** (5), 961–962.
- HENDERSON, C. B 1976 Drag coefficients of spheres in continuum and rarefied flows. *AIAA Journal* **14** (6), 707–708.
- HERMAN, HERBERT 1988 Plasma spray deposition processes. *MRS Bulletin* **13** (12), 60–67.
- HODGES, A. J. 1957 The drag coefficient of very high velocity spheres. *Journal of the Aeronautical Sciences* **24** (10), 755–758.
- HORNUNG, HANS G, SCHRAMM, JAN MARTINEZ & HANNEMANN, KLAUS 2019 Hypersonic flow over spherically blunted cone capsules for atmospheric entry. Part 1. The sharp cone and the sphere. *Journal of Fluid Mechanics* **871**, 1097–1116.
- HOWARTH, LESLIE 1948 Concerning the effect of compressibility on laminar boundary layers and their separation. *Proc. R. Soc. Lond. A* **194** (1036), 16–42.
- HUGONIOT, HENRI 1887 Memoir on the propagation of movements in bodies, especially perfect gases (first part). *J. de l'Ecole Polytechnique* **57**, 3–97.
- IMAI, I 1957 Theory of bluff bodies. *Maryland, Tech. Note. BN-104* .
- KISSEL, H. 2003 Cfd investigation of rarefied flow conditions in the test section of a low density, hypervelocity expansion tube dump tank. *Tech. Rep.* Technical Report No. 2003/08. Department of Mechanical Engineering, University of Queensland, reproduced from Ref Macrossan (2006).
- LI, CHENXI, SINGH, NARENDRA, ANDREWS, AUSTIN, OLSON, BERNARD A, SCHWARTZENTRUBER, THOMAS E & HOGAN JR, CHRISTOPHER J 2019 Mass, momentum, and energy transfer in supersonic aerosol deposition processes. *International Journal of Heat and Mass Transfer* **129**, 1161–1171.
- LIGHTHILL, MJ 1957 Dynamics of a dissociating gas part I equilibrium flow. *Journal of Fluid Mechanics* **2** (1), 1–32.
- LOTH, E 2008 Compressibility and rarefaction effects on drag of a spherical particle. *AIAA Journal* **46** (9), 2219–2228.
- MACROSSAN, MICHAEL 2006 Scaling parameters for hypersonic flow: Correlation of sphere drag data. In *Twenty-fifth Int. Symp. Rarefied Gas Dynamics, St. Petersburg, Russia*, p. 759–764.
- MANKODI, TAPAN K, BHANDARKAR, UPENDRA V & MYONG, RS 2020 Collision cross sections and nonequilibrium viscosity coefficients of N₂ and O₂ based on molecular dynamics. *Physics of Fluids* **32** (3), 036102.
- MAY, A. & WITT, W. R. 1953 Free-flight determinations of the drag coefficients of spheres. *Journal of the Aeronautical Sciences* **20** (9), 635–638.
- MILLIKAN, ROBERT A 1923 Coefficients of slip in gases and the law of reflection of molecules from the surfaces of solids and liquids. *Physical review* **21** (3), 217.
- OBLAPENKO, G & KUSTOVA, EV 2020 Influence of angular momentum on transport coefficients in rarefied gases. *Physica A: Statistical Mechanics and its Applications* p. 124673.
- OVERELL, P. 2003 Numerical simulation of rarefied flow over a hemispherical body using direct simulation monte carlo method and investigation of scaling parameters to define the flow. *Tech. Rep.*. Bachelor of Engineering thesis, School of Engineering, University of Queensland, reproduced from Ref Macrossan (2006).
- PATTERSON, GORDON N 1971 *Introduction to the kinetic theory of gas flows*. University of Toronto Press.
- PHILLIPS, WARREN F 1975 Drag on a small sphere moving through a gas. *The Physics of Fluids* **18** (9), 1089–1093.
- RANKINE, WILLIAM JOHN MACQUORN 1870 XV. On the thermodynamic theory of waves of

- finite longitudinal disturbance. *Philosophical Transactions of the Royal Society of London* (160), 277–288.
- SCHMIDT, TOBIAS, GARTNER, FRANK, ASSADI, HAMID & KREYE, HEINRICH 2006 Development of a generalized parameter window for cold spray deposition. *Acta Materialia* **54** (3), 729–742.
- SINGH, NARENDRA & AGRAWAL, AMIT 2016 Onsager’s-principle-consistent 13-moment transport equations. *Physical Review E* **93** (6), 063111.
- SINGH, NARENDRA, JADHAV, RAVI SUDAM & AGRAWAL, AMIT 2017 Derivation of stable Burnett equations for rarefied gas flows. *Physical Review E* **96** (1), 013106.
- SINGH, NARENDRA & SCHWARTZENTRUBER, THOMAS E 2016 Heat flux correlation for high-speed flow in the transitional regime. *Journal of Fluid Mechanics* **792**, 981–996.
- SINGH, NARENDRA & SCHWARTZENTRUBER, THOMAS E 2017 Aerothermodynamic correlations for high-speed flow. *Journal of Fluid Mechanics* **821**, 421.
- SREEKANTH, A. K. 1962 Drag measurement on circular cylinders and spheres in a highly rarefied gas stream at a Mach number of two. *ARS Journal* **32** (5), 748–754.
- STEWARTSON, KO 1949 Correlated incompressible and compressible boundary layers. *Proc. R. Soc. Lond. A* **200** (1060), 84–100.
- STRUCHTRUP, HENNING 2005 Macroscopic transport equations for rarefied gas flows. In *Macroscopic Transport Equations for Rarefied Gas Flows*, pp. 145–160. Springer.
- ZARIN, N. A. & NICHOLLS, J. A. 1971 Sphere drag in solid rockets—non-continuum and turbulence effects. *Combustion Science and Technology* **3** (6), 273–285.
- ZHANG, CHONGLIN, THAJUDEEN, THASEEM, LARRIBA, CARLOS, SCHWARTZENTRUBER, THOMAS E & HOGAN JR, CHRISTOPHER J 2012 Determination of the scalar friction factor for nonspherical particles and aggregates across the entire Knudsen number range by direct simulation Monte Carlo (DSMC). *Aerosol Science and Technology* **46** (10), 1065–1078.